A Parametric Power Model of Multi-Band Sub-6 GHz Cellular Base Stations Using On-Site Measurements

Louis Golard*, Youssef Agram†, François Rottenberg‡, François Quitin†, David Bol*, and Jérôme Louveaux*

*ICTEAM Institute, UCLouvain, Louvain-La-Neuve, Belgium
†Brussels School of Engineering, ULB, Brussels, Belgium
‡Faculty of Engineering Technology, KULeuven, Ghent, Belgium
Email: *{louis.golard | david.bol | jerome.louveaux}@uclouvain.be, †{youssef.agram | francois.quitin}@ulb.be,
‡francois.rottenberg@kuleuven.be

***Abstract*—The increasing energy consumption of mobile networks has emerged as a critical concern for mobile telecommunication operators, requiring measures to curb or reverse the historical upward trajectory in order to align with the sector's decarbonization target. Meanwhile, 5G-NR is massively deployed in the networks to improve quality of service, with the hope of simultaneously improving energy efficiency thanks to enhanced power-saving features. However, up-to-date 5G-enabled base stations, that support higher bandwidths with more transceivers at higher frequencies, raise concerns about their absolute power consumption, especially at low traffic loads. Proper power models are therefore needed to identify the key levers for energy savings in mobile networks under real traffic loads. This paper addresses this challenge by first providing a parametric power consumption model applicable to commercial sub-6 GHz cellular base stations. Then, numerical model parameters are estimated by combining on-site measurements from operators with radio equipment documentation from manufacturers. The uncertainty of model predictions is assessed to be in the range of 10-20%. Moreover, we show that the proposed average power model aligns well with measurements of equipment that use existing power-saving features. Estimates of power consumption are also provided for typical 3-sector single-band macro base stations in active mode, e.g., 1-4 kW when equipped with traditional radio units, and 2-4 kW when using active antenna units.**

***Index Terms*—Power consumption, Parametric power model, Base stations, On-site measurements, Power-saving features.**

I. Introduction

The radio access network (RAN) comprises a large number of base stations (BSs) that are responsible for more than 80% of the energy consumption of mobile networks [1], [2]. Moreover, historical data shows an upward trend in the RAN energy consumption, which is forecasted to continue in the future [2], [3]. In the context of climate change, this raises concerns for operators who must reduce their carbon footprint [4]. Meanwhile, 5G-NR equipment are massively deployed in the RAN to improve quality of service with the hope of improving the network energy efficiency at the same time. Indeed, 5G-NR equipment allow for enhanced power-saving features, e.g., lean carrier design, dynamic selection of antennas in massive MIMO, deep sleep modes, etc [5], [6].

This paper aims to derive a parametric model that captures the power consumption profile of up-to-date BS equipment, in order to identify the key levers for power savings in mobile networks. We also provide approximate but realistic numerical values for the model parameters, enabling quantitative comparison of different BS configurations. This work focuses on commercial BS architectures, i.e., macro and micro multi-band sub-6 GHz cellular BSs in 4G-LTE and 5G-NR.

Parametric BS power models have been covered in the literature. In [7], the authors propose a simple power model for legacy multi-band BSs. For single-band traditional BSs, references [8], [9] provide detailed model parameters using a diversity of technical data sources, while [10] uses generic power values. Other works consider massive-MIMO BSs, as [11] extending [8], and [12] focusing on energy efficiency. Future mmWave and THz systems are also studied in [13] using the same approach as in [8], [11], but are outside the scope of this work since the technology is still under development and not massively deployed yet. Besides, other works have shown a linear dependence of the average BS power consumption on traffic load [3], [14], [15], whereas sleep modes may introduce non-linear effects [3], [5], [6], [14].

However, we identify two major weaknesses in these studies. First, they generally lack to validate the numerical values they provide through real measurements. Second, it is not always clear to what time scale the models apply. Therefore, we propose a model that combines two time scales: (i) the instantaneous time scale corresponds to an OFDM symbol duration (typically 71 µs with a subcarrier spacing of 15 kHz [16]), and (ii) the average time scale corresponds to a much longer time interval (typically one hour). The instantaneous model is able to capture the non-linear behavior of the BSs and to evaluate the impacts of different power-saving features. The time-averaged version of the model is used to validate it with on-site measurements and equipment documentation.

This paper is structured as follows: Section II presents our general modeling approach, Section III details the analytical power models of main BS components, Section IV provides the estimates of numerical model parameters, Section V analyzes specific power-saving features, and Section VI discusses our results before concluding in Section VII.

II. General modeling approach

The structure of the power model is inspired from [17]. The model architecture comprises four main components: the power amplifier (PA), the analog front-end (AFE), the digital baseband (DBB) and the power supply and cooling

systems (PSC). In general, a BS may serve multiple sectors and support multiple frequency bands. We define *a cell* as being one frequency band covering one sector, e.g., a 3-sectors BS with 2 bands contains 6 cells. The power consumption of the components can be different in each of the N_C cells of the BS, depending on their configurations and operating conditions. The total BS power consumption is expressed as

$$P_{BS} = \sum_{c=1}^{N_C} \left(P_{PA,c} + P_{AFE,c} + P_{DBB,c} + P_{PSC,c} \right). \quad (1)$$

The main components comprise multiple sub-components dedicated to different signal processing steps [8]–[13], [17]. The power consumption of a given component depends on the operating conditions of its sub-components, which can vary over time. These conditions are determined by the communication protocols and the cell utilization, e.g., active downlink (DL), active uplink (UL), idle, etc. If a component contains N instances of the same sub-component, the number of sub-components in active mode is denoted by $N^{\diamond}$ (in this paper, the superscript $^{\diamond}$ refers to the active mode), while the remaining $(N{-}N^{\diamond})$ sub-components are in sleep mode. In active mode, a sub-component can switch between K active states over time. We assume that sub-components do not change their state at the instantaneous time scale, and that, on average, each active sub-component stays in each state for the same duration as the others. Therefore, the average power of an active sub-component is the arithmetic mean of its K power consumption P_k for different states k, weighted by $\tau_k = T_k/T$ the ratio of time T_k spent in that state during the time interval T. In sleep mode, the sub-component consume P_{sleep}. Overall, the average power consumption of a generic component is

$$\bar{P}(T) = \frac{1}{T} \int_0^T P(t) \mathrm{d}t = N^{\diamond} \sum_{k=1}^{K} \tau_k P_k + (N - N^{\diamond}) P_{sleep}. \quad (2)$$

In active mode, sub-components can be either in working mode or in idle. Moreover, the instantaneous working power consumption may vary depending on the sub-component usage, leading to different active states. We model the working power consumption using three static scaling features: the carrier frequency f, the maximum available bandwidth B and the maximum PA output power P_{TX}^{max}, relative to a reference situation defined by $f^{\star}$, $B^{\star}$ and $P^{\star}$. The instantaneous power consumption of specific sub-components also depends on the instantaneous load $x(t)$ in terms of physical resources (in the frequency- and spatial-domain) [5], [8]. In a multi-antenna OFDM system with N_L spatial layers, the instantaneous load of a given layer l is defined by the instantaneous number of subcarriers used to transmit data $X(l,t)$ divided by the total number of subcarriers available to transmit data $X_{DL}(l,t)$ on that layer. Then, the average physical load of a cell is the time average of instantaneous loads on all its layers as

$$\bar{x}(T) = \frac{1}{T} \int_0^T \left(\frac{1}{N_L} \sum_{l=1}^{N_L} \frac{X(l,t)}{X_{DL}(l,t)} \right) \mathrm{d}t, \quad (3)$$

meaning that the maximum achievable load is 1. In idle or in sleep mode, we model the power consumption of sub-components using reduction factors $\delta \leq 1$ with respect to their working power consumption.

To determine the useful service provided by the BS, we have to compute the actual data traffic from the physical load. To do this, we need to know the radio channel quality between the BS and mobile terminals, and derive the corresponding number of bits per subcarrier (i.e. the spectral efficiency). Yet, in this paper, we keep the physical resource load as the variable representing the service provided in the cells, in order not to depend on specific radio channel models for each BS site.

III. Analytical models of main components

A. Power amplifier

In OFDM systems, the maximum PA output power P_{TX}^{max} is lower than the PA saturation power P_{TX}^{sat} due to the high peak-to-average power ratio $P_{TX}^{sat}/P_{TX}^{max} > 1$ that requires a significant output power back-off (OPBO). With an adaptive supply, the full-load output power P_{TX}^{full} can also be set lower than P_{TX}^{max}. We propose to model the instantaneous power consumption of a single active PA by the sum of a static power proportional to P_{TX}^{max} and a dynamic power that scales with the instantaneous output power $p(t) \leq P_{TX}^{full}$. In general, this scaling is non-linear with an efficiency that increases with p as $\eta_{PA} = \eta_{PA}^{max} \cdot \left(p / P_{TX}^{full} \right)^n$, where η_{PA}^{max} is the PA efficiency at P_{TX}^{max} and $n \in [0,1]$, as discussed in [18]–[20]. This leads to

$$P_{PA}(p(t)) = \xi \frac{P_{TX}^{max}}{\eta_{PA}^{max}} + (1-\xi) \frac{\left(P_{TX}^{full} \right)^n \left(p(t) \right)^{1-n}}{\eta_{PA}^{max}}, \quad (4)$$

with $\xi \in [0,1]$ the ratio of static to maximum power consumption. The full-load PA efficiency is hence lower than η_{PA}^{max}, except if $P_{TX}^{full} = P_{TX}^{max}$ in which case it equals to η_{PA}^{max}. In Table I, we use [18]–[22] to propose theoretical (ranges of) parameter values suited to (4) for five common PA architectures, considering the typical 8 dB OPBO for LTE and NR.

Moreover, the maximum PA efficiency is limited by power losses in the transistors, that can be either frequency-dependent or independent, as explained in [21], [22]. We model this by

$$\eta_{PA}^{max} = \frac{\eta_{PA}^{tech}}{1 + a \cdot \left(\frac{P_{TX}^{max}}{P^{\star}} \right) \left(\frac{f}{f^{\star}} \right)^2 + b \cdot \left(\frac{P^{\star}}{P_{TX}^{max}} \right)}, \quad (5)$$

where η_{PA}^{tech} is the highest achievable efficiency for a given PA architecture and technology, and a and b are dimensionless technology-specific parameters. This model states that η_{PA}^{max} deteriorates as frequency increases for a fixed P_{TX}^{max}, whereas, for a fixed frequency, it first increases, then peaks and finally decreases as P_{TX}^{max} increases.

TABLE I
Theoretical model parameters for common PA architectures

Architecture	ξ	n	η_{PA}^{max}
Class-A	1	1	0.08
Class-B	0	0.5	0.31
Class-AB	$]0,1[$	0.5	$]0.08, 0.31[$
Envelope tracking	$]0,1[$	0	$]0.08, 0.79[$
Doherty	$]0,1[$	$]0, 0.5[$	$]0.08, 0.79[$

The average PA power consumption can be expressed by using (2). Based on [5], we assume 4 different active states for the $N_{PA}^{\diamond}$ active PAs:

- DL mode and full-load data transmission at $p = P_{TX}^{full}$,
- DL mode and reference signal transmission only at $p = P_{TX}^{sig} = \zeta_{sig} P_{TX}^{full}$, ζ_{sig} denoting the signaling power ratio,
- DL mode and no transmission such that $p = 0$,
- Idle mode when the PA is not in DL mode, with $p = 0$

The time ratio of the DL mode is τ_{DL} and varies depending on the duplex mode: $\tau_{DL} = 1$ in frequency division duplex (FDD), and $\tau_{DL} < 1$ in time division duplex (TDD). The time ratio of the idle mode is its counterpart, i.e., $(1-\tau_{DL})$. Since we consider a single data transmission state during which all physical resources are used at full output power, the instantaneous load $x(t)$ can be either 0 or 1, which is compatible with current BS operation under real traffic loads. Hence, the time ratio in this state is proportional to the average load as $\tau_{DL}\bar{x}(T)$. When no data is transmitted in DL mode, the BS keeps on transmitting reference signals during $\tau_{sig}\tau_{DL}\cdot(1-\bar{x}(T))$, with τ_{sig} the time ratio of reference signal transmission. The PA power consumptions in DL without transmission, in idle and in sleep mode are modeled using reduction factors δ_{PA}^{dtx}, δ_{PA}^{idle} and δ_{PA}^{sleep}, respectively. The average PA power consumption is then given by a weighted sum of its power in the five states:

$$\begin{aligned}\bar{P}_{PA}(T) = \\ N_{PA}^{\diamond}\cdot\Big[&\bar{x}(T)\tau_{DL}P_{PA}(P_{TX}^{full}) + (1-\bar{x}(T))\tau_{sig}\tau_{DL}P_{PA}(P_{TX}^{sig}) \\ &+(1-\bar{x}(T))(1-\tau_{sig})\tau_{DL}P_{PA}(0)\delta_{PA}^{dtx} + (1-\tau_{DL})P_{PA}(0)\delta_{PA}^{idle}\Big] \\ &+(N_{PA}-N_{PA}^{\diamond})P_{PA}(0)\delta_{PA}^{sleep}, \end{aligned} \tag{6}$$

which is linear with respect to the load, in line with [3], [15].

B. Analog front-end

The AFE contains M sub-components performing specific analog functions in transmission (TX), i.e., digital-to-analog conversion, up-conversion and pre-driving, in reception (RX), i.e., low-noise amplification, down-conversion and analog-to-digital conversion, and for the whole cell, i.e., frequency synthesis, clock generation and general control [8]–[13]. Unlike for the PA, the instantaneous power consumed to perform these functions is assumed independent of the load so that active AFE sub-components can only be in two active states: working mode or idle. The working power consumption of a sub-component i is modeled as in [8] using a reference power P_i^{ref} that scales with a set of S scaling features having each a reference value $y_j^{\star}$, an actual value y_j, and a specific scaling exponent α_{ij} with respect to feature j:

$$P_i = P_i^{ref}\prod_{j=1}^{S}\left(\frac{y_j}{y_j^{\star}}\right)^{\alpha_{ij}}. \tag{7}$$

To limit the number of parameters in the AFE model, we propose the following simplifications:

- the AFE functions are aggregated to consider only three sub-components, namely the TX chain, the RX chain and the other miscellaneous functions, leading to $M = 3$,
- the working mode of a TX (resp., RX) chain is the DL (resp., UL) mode, while the miscellaneous functions are always in working mode when the cell is active,
- the scaling features are limited to B and P_{TX}^{max} for TX and RX chains, and to B and the total cell output power $P_{TX}^{cell} = N_{PA}P_{TX}^{max}$ (i.e., a proxy for the AFE size) for miscellaneous functions, leading to $S = 2$ in all cases,
- the same reference powers, scaling exponents and reduction factors are used for the TX and RX chains.

By (7), the working power consumptions of the miscellaneous functions and of one TX or RX chain are respectively:

$$P_{misc} = P_{misc}^{ref}\cdot\left(\frac{B}{B^{\star}}\right)^{\alpha_{11}}\left(\frac{P_{TX}^{cell}}{P^{\star}}\right)^{\alpha_{12}} \tag{8}$$

$$P_{TXc} = P_{RXc} = P_{TRX} = P_{TRX}^{ref}\cdot\left(\frac{B}{B^{\star}}\right)^{\alpha_{21}}\left(\frac{P_{TX}^{max}}{P^{\star}}\right)^{\alpha_{22}}. \tag{9}$$

The total power consumed by the AFE is the sum of all sub-component contributions. Assuming that the number of installed (resp., active) TX and RX chains are equal in a cell, denoted by N_{TRX} (resp., $N_{TRX}^{\diamond}$), the average AFE power consumption is obtained by combining (2), (8) and (9) as

$$\begin{aligned}\bar{P}_{AFE}(T) = P_{misc}\cdot&\Big[N_B^{\diamond} + (N_B - N_B^{\diamond})\delta_{misc}^{sleep}\Big] \\ &+P_{TRX}\cdot\Bigg[N_{TRX}^{\diamond}\cdot\Big((\tau_{DL}+\tau_{UL})+(2-\tau_{DL}-\tau_{UL})\delta_{TRX}^{idle}\Big) \\ &+2\cdot(N_{TRX}-N_{TRX}^{\diamond})\,\delta_{TRX}^{sleep}\Bigg], \end{aligned} \tag{10}$$

where N_B and $N_B^{\diamond}$ denote respectively the number of installed and active bands in the cell. Since we defined that a cell consists of a single band, $N_B = 1$.

C. Digital baseband

The DBB performs digital functions such as physical resource scheduling, coding, modulation, digital precoding and/or beamforming, decoding, demodulation, etc [8]–[13]. The DBB power consumption is assumed to be load-independent, as it is commonly observed [14], [15]. In a given cell, it is modeled by the sum of powers related to the data link layer P_{link} and to the physical layer P_{phy}. The former is considered to scale with the inverse of the total number of cells in the BS, while the latter is modeled using the same approach as of AFE sub-components, i.e. we assume the same states, and the working power is also modeled by (7) considering the bandwidth as the unique scaling feature. The number of active spatial layers is denoted by $N_L^{\diamond}$. Using (2), we obtain

$$\begin{aligned}\bar{P}_{DBB}(T) = \frac{P_{link}^{ref}}{(N_C)^{\alpha_3}} + P_{phy}^{ref}\cdot\left(\frac{B}{B^{\star}}\right)^{\alpha_4}&\Bigg[N_L^{\diamond}\cdot\Big((\tau_{DL}+\tau_{UL}) \\ &+(2-\tau_{DL}-\tau_{UL})\delta_{phy}^{idle}\Big) + 2\cdot(N_L-N_L^{\diamond})\,\delta_{phy}^{sleep}\Bigg]. \end{aligned} \tag{11}$$

D. Power supply and cooling systems

In addition to previous components, the BS also includes power supply and cooling modules comprising power converters (AC/DC and DC/DC) and active cooling, introducing additional power consumption [8]–[13]. We consider the overhead from the converters to linearly scale with the total power

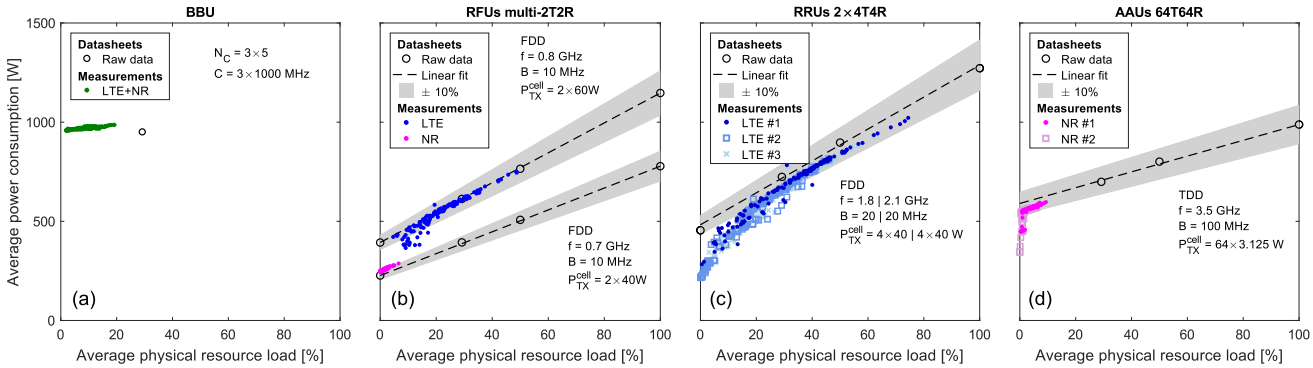

Fig. 1. Average power consumption vs. physical load for of a 3-sector macro-BS with (a) one BBU, (b) two multi-sector RFUs, (c) three dual-band RRUs, and (d) three AAUs (one is not shown due to lack of measurements). On-site measurements are compared with datasheet values, indicating a close match.

consumption with an efficiency η_{supply}, and the overhead from the cooling system to scale with the power of other main components with efficiencies η_{cool}^{PA}, η_{cool}^{AFE} and η_{cool}^{DBB}. These efficiencies are in general lower than 1, but $\eta_{cool} = 1$ if no active cooling is required. As cooling efficiencies are not necessarily the same for all components nor for all cells, the total BS power consumption given by (1) becomes:

$$P_{BS} = \frac{1}{\eta_{supply}} \sum_{c=1}^{N_C} \left(\frac{P_{PA,c}}{\eta_{cool,c}^{PA}} + \frac{P_{AFE,c}}{\eta_{cool,c}^{AFE}} + \frac{P_{DBB,c}}{\eta_{cool,c}^{DBB}} \right). \quad (12)$$

IV. Numerical Values of Model Parameters

A. Physical implementation of model components

In macro- and micro-BSs, the physical implementation of the main components of the model consists in a power supply unit (PSU) for power converters, a baseband unit (BBU) for DBB components of up to several cells plus a cooling system, and a radio unit (RU) for AFE and PAs of one or more cells, sometimes with an active cooling system. For smaller BSs (pico and femto emitting up to 1 W per cell), all components are usually grouped together in a single unit, but these BS types are not considered in this work. RUs can also be split into several subcategories: macro RU emitting from 40 W to several hundred watts per cell or micro RU (μRU) emitting 1 to 20 W per cell, RU supporting FDD or TDD, radio frequency unit (RFU) installed in the BS cabinet, remote radio unit (RRU) installed closer to passive antennas, or active antenna unit (AAU) combining AFE, PAs and antenna elements in a single unit. In general, BBUs and RUs are able to support different protocols such as LTE and NR, and sometimes both at the same time. However, specific equipment is usually optimized for one of the two (e.g. AAU at 3.5 GHz for NR).

B. Data sources

Parameters estimation relies on two types of data sources:

- on-site measurements from different operators,
- equipment documentation from different manufacturers.

On-site physical counters provide hourly average measurements (e.g., the power consumption, the physical load, the number of connected users) of operating BS components, as explained in [3]. The strength of such measurements is to provide values close to reality across a range of realistic loads. Yet, the main limitation of this approach is that we only had access to measurements from a limited number of sites with a few configurations that are, in addition, time-consuming to analyze. In contrast, equipment documentation such as technical datasheets covers a much wider range of equipment, with various feature configurations $\{f, B, ...\}$ and operating conditions $\{P_{TX}^{full}, N_{TRX}^{\diamond}, x(t), ...\}$. In this work, we use datasheets of more than a hundred pieces of equipment. Another advantage of the documentation is that it provides power consumption at full load, which is never reached in normal network use. The drawback is that the given power consumptions are usually limited to four reference load levels $\bar{x} = \{0\%, 30\%, 50\%, 100\%\}$, as standardized by [23]. For confidentiality reasons, our raw dataset cannot be published.

Fig. 1 shows an example of hourly on-site measurements over one week in 2023 for an up-to-date 3-sector macro-BS deployed in a large city in Belgium. This site is equipped with RFUs, RRUs and AAUs, and supports three bands in LTE (i.e., 0.8, 1.8 and 2.1 GHz) and two bands in NR (i.e., 0.7 and 3.5 GHz). For each piece of equipment, measurements of average power consumption are plotted against the average physical load. On top of that, we display the power consumption given by the datasheets, indicating that the actual behavior of equipment matches the datasheet values when the average load is above 10-30%, with a $\pm 10\%$ tolerance. This gives us good confidence in the equipment documentation for estimating model parameters in addition to on-site measurements.

Fig. 1 also illustrates that, for RUs, a non-linear behavior appears at low-load, while at higher load their average power varies linearly with the load, in line with (6) and (10). This arises from the adaptation of their configurations with respect to the load, as detailed in Section V. For the BBU, the power consumption barely varies with the load, in line with (11), and no obvious sleep mode is observed. Finally, we note that the static power of RUs is significant, and even dominant for AAUs which was lightly loaded in 2023. As a result, their energy efficiency at low load is quite low, underlining the importance to implement power-saving features.

C. Parameter values estimation

The BS power consumption depends on the configuration of its features (e.g., f, B, N_{TRX}) which can be chosen by

TABLE II
NUMERICAL ESTIMATES OF MODEL PARAMETERS

	Parameter	Value[1]	References[2]
Ref.	$f^\star$	1 GHz	n.a.
	$B^\star$	1 MHz	n.a.
	$P^\star$	1 W	n.a.
PA	ξ	0.12 | 0.12 (AAU)	–
	n	0.25	[19], [20]
	η_{PA}^{tech}	0.38 | 0.38 (AAU)	–
	a	$\sim 10^{-4}$	[21], [22], [24]
	b	~ 1	[21], [22], [24]
	$\{\delta_{PA}^{dtx}, \delta_{PA}^{idle}, \delta_{PA}^{sleep}\}$	$\{1, 0.25, 0\}$	–
AFE	P_{misc}^{ref}	22 W | 17 W (AAU)	–
	$\{\alpha_{11}, \alpha_{12}\}$	$\{0, 0.25\}$	[8], [11]
	δ_{misc}^{sleep}	0.75	–
	P_{TRX}^{ref}	0.18 W | 0.18 W (AAU)	–
	$\{\alpha_{21}, \alpha_{22}\}$	$\{0.5, 0.5\}$	[8], [11]
	$\{\delta_{TRX}^{idle}, \delta_{TRX}^{sleep}\}$	$\{1, 0.5\}$	–
DBB	P_{link}^{ref}	90 W	–
	P_{phy}^{ref}	0.07 W	–
	$\{\alpha_3, \alpha_4\}$	$\{0.5, 1\}$	[8], [11]
	$\{\delta_{phy}^{idle}, \delta_{phy}^{sleep}\}$	$\sim\{0.75, 0.75\}$	–
PSC	η_{supply}	~ 0.90	[8], [25]
	η_{cool}^{PA}	~ 0.90	[8]
	η_{cool}^{AFE}	~ 0.90	[8]
	η_{cool}^{BB}	~ 0.95	[8]
Protocol	τ_{DL}	1.00 (FDD) | 0.75 (TDD)	[16], [26]
	τ_{UL}	1.00 (FDD) | 0.25 (TDD)	[16], [26]
	τ_{sig}	2/7 (LTE) | 1/14 (NR)	[16], [27]
	ζ_{sig}	2/6 (LTE) | 1/12 (NR)	[16], [27]

[1] Values with higher uncertainty indicated with a "$\sim$"
[2] Additional references to this work's data sources for estimating values

the network operators, and on operating conditions (e.g., the traffic load) imposed by network users. In this section, we seek to estimate the other model parameters that depend on the technology and that are not controlled by the operators nor the users. This corresponds to a parametric regression analysis for which we define $\boldsymbol{\rho}$ the vector of actual consumed power of all equipment configurations in our dataset, $\boldsymbol{\phi}$ their respective feature configurations and operating conditions, and $F(\boldsymbol{\phi}, \boldsymbol{\theta})$ the power model that depends on $\boldsymbol{\phi}$ and on $\boldsymbol{\theta}$ the parameters to estimate. This leads to a non-linear least-squares problem:

$$\hat{\boldsymbol{\theta}} = \arg\min_{\boldsymbol{\theta}} \left\{ \|\boldsymbol{\rho} - F(\boldsymbol{\phi}, \boldsymbol{\theta})\|_2^2 \right\}. \quad (13)$$

Before solving, we split our dataset into three equipment categories: BBUs, traditional RUs and AAUs, assuming comparable equipment in each category. All equipment belong to a similar technological generation and were available on the market in 2023. We then assume that $N_{PA} = N_{TRX}$ in all RUs, that $N_L = N_{TRX}$ in traditional RUs, and that $N_L < N_{TRX}$ in AAUs, in order to benefit from beamforming.

Two issues then arise: (i) there are numerous possible configurations but a limited configuration diversity in the dataset, and (ii) we try to estimate some parameters relative to the instantaneous model based on average data only. We therefore use additional references to constrain certain parameters that we try to estimate. For instance, we set $\delta^{idle} \geq \delta^{sleep}$ for the sake of consistency. We also restrict scaling exponents to specific values, such that $\alpha \in \{0, 0.25, 0.5, 0.75, 1\}$. Based

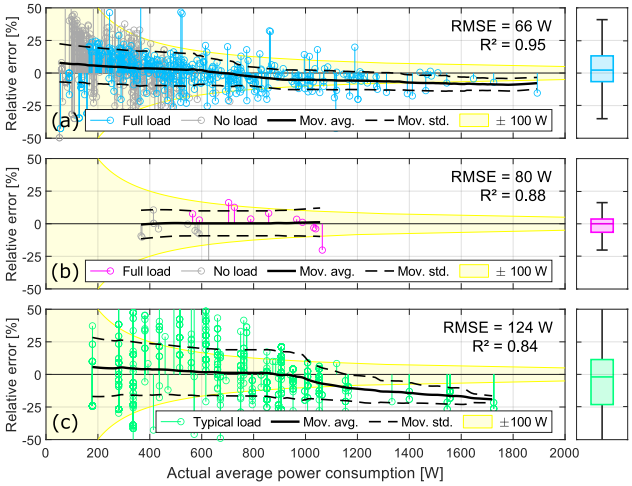

Fig. 2. Relative errors of model predictions vs. actual power consumption for (a) traditional RUs, (b) AAUs, and (c) BBUs. The yellow region indicates the zone where the absolute uncertainty is less than 100 W. Boxplots of the relative errors are displayed on the right of each graph.

on [8], [11], we then set the scaling exponents of P_{misc}, P_{TX}^{cell}, P_{TRX}, P_{link}, and P_{phy} with respect to their scaling features.

Numerical estimates of the model parameters are given in Table II. We obtain the same η_{PA}^{tech} and ξ for traditional RUs and for AAUs, even though we estimate these parameters separately. This indicates that PA technologies are similar. In fact, this corresponds to the behavior of LDMOS Doherty amplifiers, in line with [9], [12], [21], [22]. Besides, parameter values may change for other architectures, technologies, and protocols. For instance, using the micro-DTX feature on the OFDM symbol time scale [6] improves the associated reduction factors such that $\delta_{PA}^{dtx} < 1$. We might also expect technologies to improve over time [8], [13], but we caution that simplistic forecasts can lead to significant errors.

Finally, we assess the model accuracy by computing the relative errors of its predictions (i.e., $(\hat{\rho} - \rho)/\rho$) for all equipment configurations (see Fig. 2). The mean and standard deviation of relative errors, namely the bias and the uncertainty, are respectively 4% and $\pm 17\%$ for traditional RUs, -2% and $\pm 11\%$ for AAUs, and -3% and $\pm 21\%$ for BBUs. We tolerate a reasonable degree of uncertainty as we try to keep the analytical model simple and built on interpretable parameters. We note that our model overestimates the power consumption of RUs and BBUs at low power, and underestimates it at high power. One reason is the selection of scaling exponents from a discrete number of values, which limits fine-tuning.

D. Typical base station configurations

Although we aimed to develop a model applicable to a broad range of BS configurations, it does not apply, e.g., to pico or femto-BSs, or to mmWave and beyond. In Table III we then propose 8 typical BS configurations among the most common ones in our dataset. We indicate the range of configurations in which our estimates apply in the first row of the table. We consider all configurations with $N_S = 3$ sectors and $N_B = 1$ band, except for 2×4T4R which supports 2 bands. In all cases, $N_C = N_S \times N_B$. The active cooling only applies to BBUs and

TABLE III
TYPICAL BASE STATION CONFIGURATIONS

Config. name	RU type	Duplex	Protocol	$N_S \times N_B$	N_{TRX} [1]	N_L [1]	f [GHz]	B [MHz]	P_{TX}^{max} [W] [2]	P_{TX}^{full} [W] [2]	C [MHz] [3]	P_{TX}^{cell} [W] [3]
applicability	n.a.	FDD/TDD	LTE/NR	1–30	1–64	1–16	0-6	10–200	1–80	1–80	10–3200	5–500
micro-4T4R	µRRU	FDD	LTE	3×1	4	4	1.8	20	5	5	80	20
multi-2T2R	RFU	FDD	LTE	3×1	2	2	0.8	20	80	80	40	160
2T2R	RRU	FDD	LTE	3×1	2	2	1.8	20	80	40	40	160
4T4R	RRU	FDD	LTE	3×1	4	4	1.8	20	40	40	80	160
2×4T4R	RRU	FDD	LTE	3×2	4 | 4	4 | 4	1.8 | 2.1	20 | 20	40 | 40	40 | 40	80 | 80	160 | 160
8T8R	RRU	TDD	NR	3×1	8	8	3.5	100	40	40	800	320
32T32R	AAU	TDD	NR	3×1	32	8	3.5	100	6.25	6.25	800	200
64T32R	AAU	TDD	NR	3×1	64	8	3.5	100	3.125	3.125	800	200

[1] Parameters given per cell [2] Parameters given per PA (and hence per TX chain) [3] Resulting configurations per cell

RFUs, whereas $\eta_{cool} = 1$ for RRUs and AAUs. The multi-sectors 2T2R (multi-2T2R) configuration is special because a single RFU supports all the 3 sectors of the BS, so that the power model must be adapted with $\tilde{P}_{misc} = P_{misc}/3$ and $\tilde{P}_{TX}^{cell} = 3P_{TX}^{cell}$. These typical configurations can be combined to obtain practical BS configurations, such as the one shown in Fig. 1. The last two columns of Table III provide the resulting cell capacity $C = N_L B$ and total cell output power. This gives an idea of the service offered by each BS configuration, since the capacity is proportional to the total amount of physical resources available for DL, influencing the achievable peak data throughput, and as P_{TX}^{cell} determines the cell coverage. These aspects must be considered to ensure a fair comparison between BS configurations.

Fig. 3 shows the total power consumption of typical BS configurations, broken down by model components and sub-components. The PA induces most of the load-dependent power consumption, along with the PSC. In LTE, the impact of signaling is visible in the dynamic PA power, which is no longer the case in NR thanks to less-frequent signaling [5], [6]. At full load, the PA power dominates in most configurations, although AFE power becomes significant as N_{TRX} and B increase, especially for AAUs. DBB power also increases with N_L and B, but remains small compared to the total BS power. Yet, the share of DBB power could rise for small mmWave BSs, emitting less power but using wider bandwidths.

V. POWER-SAVING FEATURES

The non-linear effects at low and no load observed in Fig. 1 can be attributed to specific power-saving features that adapt dynamically the BS configuration to the load, e.g., $N_{TRX}^{\diamond}(x(t))$, $N_{PA}^{\diamond}(x(t))$ or $P_{TX}^{full}(x(t))$. Here, we discuss the implementation of such techniques based on [5]:

- time-domain technique: switching of components from working to idle or sleep mode, as modeled in Section II,
- frequency-domain technique: deactivation of a half or full frequency band,
- spatial-domain technique: deactivation of half of the layers and of the corresponding PAs and TX/RX chains.

No power-domain techniques are involved here, but all the above techniques lead to a reduction in output power P_{TX}^{full} for specific PAs, or even to switch them off. Layer or (half) band deactivation also leads to reduction in available capacity.

In Fig. 4, we focus on the dual-band 4T4R RRUs. We first represent the average power model with different combinations of power-saving features corresponding to RRU configurations that are fixed over time and provide 75%, 50%, 25% and 0% of total capacity. This shows that, for a given active capacity,

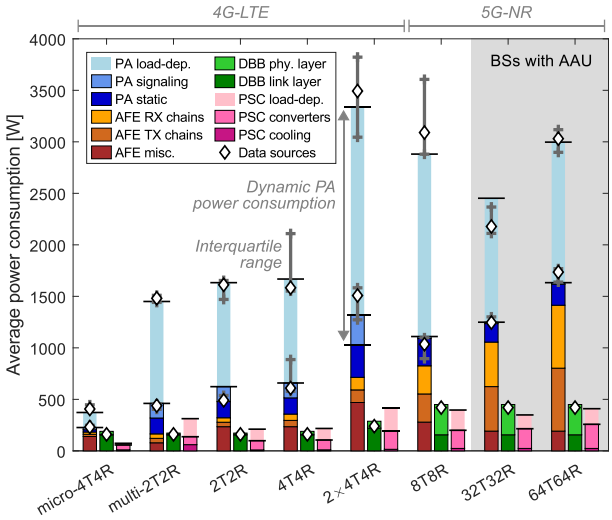

Fig. 3. Power consumption breakdown of typical BS configurations in active mode. The median and interquartile range of power given by data sources are displayed at full and no load for PA+AFE, and at typical load for DBB.

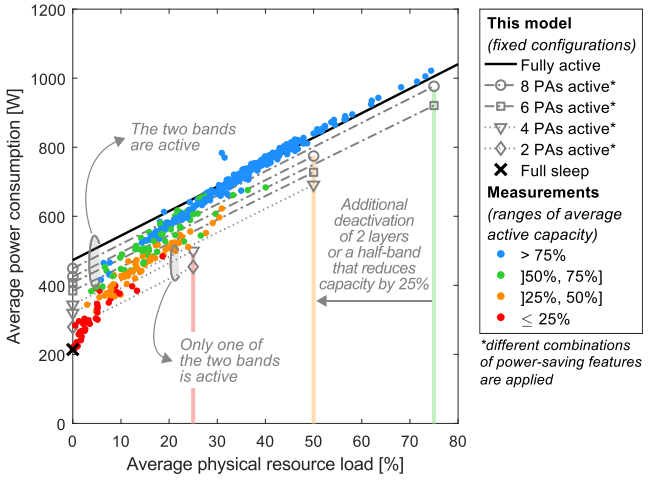

Fig. 4. Average power vs. load when using power-saving features in the RRUs 2×4T4R. The average model is displayed for fixed configurations, while measurements are classified by range of average active capacity.

the RRU consumes more power when more PAs and TX/RX chains are active, even if they are individually less loaded. We then superimpose on-site measurements categorized by range of average active capacity, as power-saving states may change during the measurement interval. Comparing these measurement categories with corresponding model predictions reveals a close alignment between them. This indicates that our average model can be used to study power-saving strategies at the system level. Yet, the instantaneous model must be used to assess the impact of these strategies on communication performance, e.g., the peak or user experienced throughput.

VI. Discussion

Compared with the popular flexible model in [8], we found, for typical macro-BSs with traditional RUs, +20-40% higher power consumption at full load, and +40-60% at no load. The difference is significantly larger for BSs with AAUs, as [11] predicts power consumption 5-20$\times$ lower than our model. This raises questions about the suitability of existing models in the literature for planning and optimization of future RAN deployment. However, our modeling approach also has limitations due to the use of commercial equipment with heterogeneity in designs, architectures and technologies, even for comparable products. This induces uncertainty in the estimated numerical values and affects the model accuracy. The proposed BS power breakdown is also uncertain as we did not measure the power consumption of the sub-components separately. In addition, we cannot guarantee absolute representativeness of all existing BS equipment as we studied only a sample of commercially available equipment. Nevertheless, we think that the datasets we used are quite robust, and we believe that this work, which is based on on-site measurements, will be useful for updating BS power models in the literature.

VII. Conclusion

This paper presents a parametric power model for multi-band sub-6GHz cellular BSs, along with numerical parameter estimates. The model is built around four main components and cover both instantaneous and average time scales. The model has proven its reliability by (i) providing accurate power consumption estimates for typical BS configurations, and (ii) capturing power-saving features currently deployed, both matching with on-site measurements. We found that power consumption of commercial BS is actually higher than predicted by existing models in the literature, especially for AAUs. Therefore, it points out the need to implement enhanced power-saving features to reduce their operating power when lightly loaded, as they consume high static power when fully active. Furthermore, we remind that a life-cycle perspective is needed to assess all the environmental impacts of a BS, meaning that we should consider, e.g., their manufacturing, maintenance and end-of-life, in addition to their energy consumption that models their use phase only.

Acknowledgment

The authors would like to thank Proximus and MWingz for their support. This work was partly funded by Proximus.

References

[1] D. Lundén, J. Malmodin, P. Bergmark and N. Lövehagen, "Electricity consumption and operational carbon emissions of european telecom network operators," *Sustainability*, 2022.
[2] L. Stobbe, N. Richter, M. Quaeck et al., "Umweltbezogene technikfolgenabschätzung mobilfunk in Deutschland," Umweltbundesamt, 2023.
[3] L. Golard, J. Louveaux and D. Bol, "Evaluation and projection of 4G and 5G RAN energy footprints: The case of Belgium for 2020–2025," *Ann. Telecommun.*, 2023.
[4] ITU-T Recommendation L.1470, "Greenhouse gas emissions trajectories for the information and communication technology sector compatible with the UNFCCC Paris Agreement," 2020.
[5] T. Islam, D. Lee and S. S. Lim, "Enabling network power savings in 5G-Advanced and beyond," *IEEE J. Sel. Areas Commun.*, 2023.
[6] F. E. Salem, T. Chahed, Z. Altman and A. Gati, "Traffic-aware advanced sleep modes management in 5G networks," in *IEEE Wireless Commun. Netw. Conf.*, 2019.
[7] J. Lorincz and T. Matijevic, "Energy-efficiency analyses of heterogeneous macro and micro base station sites," *Comput. Electr. Eng.*, 2014.
[8] B. Debaillie, C. Desset and F. Louagie, "A flexible and future-proof power model for cellular base stations," in *IEEE 81st Veh. Technol. Conf.*, 2015.
[9] W. Wang, D. Liu, Y. Zhang and C. Gong, "Energy estimation and optimization platform for 4G and the future base station system early-stage design," *China Commun.*, 2017.
[10] B. H. Jung, H. Leem and D. K. Sung, "Modeling of power consumption for macro-, micro-, and RRH-based base station architectures," in *IEEE 79th Veh. Technol. Conf.*, 2014.
[11] C. Desset, B. Debaillie and F. Louagie, "Modeling the hardware power consumption of large scale antenna systems," in *IEEE Online Conf. Green Commun.*, 2014.
[12] E. Björnson, L. Sanguinetti, J. Hoydis and M. Debbah, "Optimal design of energy-efficient multi-user MIMO systems: Is massive MIMO the answer?," *IEEE Trans. Wireless Commun.*, 2015.
[13] C. Desset, P. Wambacq, Y. Zhang et al., "A flexible power model for mm-wave and THz high-throughput communication systems," in *IEEE 31st Int. Symp. Pers., Indoor, Mobile Radio Commun.*, 2020.
[14] G. Auer, V. Giannini, C. Desset et al., "How much energy is needed to run a wireless network?," *IEEE Wireless Commun.*, 2011.
[15] A. Capone, S. D'Elia, I. Filippini et al., "Modeling energy consumption of mobile radio networks: An operator perspective," *IEEE Wireless Commun.*, 2017.
[16] 3GPP Technical Specification TS 36.211 V17.4.0, "Radio access network; Evolved universal terrestrial radio access (E-UTRA); Physical channels and modulation (release 17)," 2023.
[17] C. Desset, B. Debaillie and F. Louagie, "Towards a flexible and future-proof power model for cellular base stations," in *24th Tyrrhenian Int. Workshop Digit. Commun.*, 2013.
[18] F. Rottenberg, "Information-theoretic study of time-domain energy-saving techniques in radio access," *arXiv preprint*, 2023.
[19] A. Hossain and R. Jäntti, "Impact of efficient power amplifiers in wireless access," in *IEEE Online Conf. Green Commun.*, 2011.
[20] J. Joung, C. Ho and S. Sun, "Spectral efficiency and energy efficiency of OFDM systems: Impact of power amplifiers and countermeasures," *IEEE J. Sel. Areas Commun.*, 2014.
[21] F. van Rijs and S. Theeuwen, "Efficiency improvement of LDMOS transistors for base stations: towards the theoretical limit," in *Int. Electron Devices Meet.*, 2006.
[22] S. Theeuwen and J. Qureshi, "LDMOS technology for RF power amplifiers," *IEEE Trans. Microw. Theory Tech.*, 2012.
[23] ETSI Standard ES 202 706-1 V1.7.1, "Metrics and measurement method for energy efficiency of wireless access network equipment; Part 1: Power consumption - static measurement method," 2022.
[24] H. Wang, K. Choi, B. Abdelaziz et al., "Power amplifiers performance survey 2000-present," https://ideas.ethz.ch/research/surveys/pa-survey.html, 2023.
[25] C. Yan, Y. Ye, J. Ying and B. Blair, "Design considerations of high efficiency high density telecom rectifier," in *IEEE Int. Telecommun. Energy Conf.*, 2010.
[26] 3GPP Technical Specification TS 38.213 V18.1.0, "Radio access network; NR; Physical layer procedures for control (release 18)," 2023.
[27] 3GPP Technical Specification TS 38.211 V18.1.0, "Radio access network; NR; Physical channels and modulation (release 18)," 2023.